crystals

MDPI

Article

Rapid Aqueous-Phase Synthesis and Photoluminescence Properties of $K_{0.3}Bi_{0.7}F_{2.4}$:Ln^{3+} (Ln = Eu, Tb, Pr, Nd, Sm, Dy) Nanocrystalline Particles

Weili Wang, Shihai Miao *, Dongxun Chen * and Yanjie Liang *

Key Laboratory for Liquid-Solid Structure Evolution and Processing of Materials, Ministry of Education, Shandong University, Jinan 250061, China; wangweili@sdu.edu.cn

* Correspondence: 202020485@mail.sdu.edu.cn (S.M.); 202120530@mail.sdu.edu.cn (D.C.); yanjie.liang@sdu.edu.cn (Y.L.)

Abstract: Trivalent lanthanides (Ln^{3+}) doped bismuth-based inorganic compounds have attracted considerable interest as promising candidates for next-generation inorganic luminescent materials. Here, a series of $K_{0.3}Bi_{0.7}F_{2.4}$ (KBF) nanocrystalline particles with controlled morphology have been synthesized through a low-temperature aqueous-phase precipitation method. Using KBF as the host matrix, Eu^{3+}, Tb^{3+}, Pr^{3+}, Nd^{3+}, Sm^{3+}, and Dy^{3+} ions are introduced to obtain $K_{0.3}Bi_{0.7}F_{2.4}$:Ln^{3+} (KBF:Ln) nanophosphors. The as-prepared KBF:Ln nanophosphors exhibit commendable photoluminescence properties, in which multicolor emissions in a single host lattice can be obtained by doping different Ln^{3+} ions when excited by ultraviolet light. Moreover, the morphology and photoluminescence performance of these nanophosphors remain unchanged under different soaking times in water, showing good stability in a humid environment. The proposed simple and rapid synthesis route, low-cost and nontoxic bismuth-based host matrix, and tunable luminescent colors will lead the way to access these KBF:Ln nanophosphors for appealing applications such as white LEDs and optical thermometry.

Keywords: $K_{0.3}Bi_{0.7}F_{2.4}$; nanophosphors; lanthanide; photoluminescence

check for updates

Citation: Wang, W.; Miao, S.; Chen, D.; Liang, Y. Rapid Aqueous-Phase Synthesis and Photoluminescence Properties of $K_{0.3}Bi_{0.7}F_{2.4}$:Ln^{3+} (Ln = Eu, Tb, Pr, Nd, Sm, Dy) Nanocrystalline Particles. *Crystals* **2022**, *12*, 963. https://doi.org/10.3390/cryst12070963

Academic Editors: Alessandra Toncelli and Željka Antić

Received: 17 June 2022
Accepted: 8 July 2022
Published: 10 July 2022

Publisher's Note: MDPI stays neutral with regard to jurisdictional claims in published maps and institutional affiliations.

Copyright: © 2022 by the authors. Licensee MDPI, Basel, Switzerland. This article is an open access article distributed under the terms and conditions of the Creative Commons Attribution (CC BY) license (https://creativecommons.org/licenses/by/4.0/).

1. Introduction

Inorganic luminescent nanoparticles have aroused tremendous attention compared with their bulk counterparts owing to their unique features such as tunable emission peaks, sharp emission bandwidth, large stokes shift, and excellent luminescence stability against heat and irradiation [1–4]. As a result, trivalent lanthanides doped inorganic nanoparticles show a rather wide range of applications in areas such as spectroscopic analysis, anti-counterfeiting, biomedicine, and light-emitting diodes (LEDs) [5–9]. In the past two decades, a large number of novel luminescent nanomaterials have been designed and developed to take advantage of their nanoscale size and distinct luminescence properties. Among them, rare earth fluorides are becoming a hot research topic in consideration of their high chemical stability, very low lattice phonon energy, and good accommodation for Ln^{3+} [10–15]. Nevertheless, substantial rare earth salts are usually required to synthesize these rare earth fluoride nanomaterials, which greatly limits their further development and application. Therefore, it is urgent and necessary to further explore new and efficient host materials for luminescent lanthanides.

Bismuth-based inorganic materials are considered promising candidates for developing the next-generation inorganic phosphors because of the advantages of the relatively inexpensive, nontoxic, and unique electronic structure of bismuth elements [16–19]. Among these bismuth-based inorganic hosts, bismuth fluorides have attracted significant attention [20,21]. As a result of extensive research, lanthanide-doped bismuth fluorides have been found numerous applications in photocatalysis (e.g., BiOF:Eu^{3+} and

$Bi_7O_5F_{11}$:Eu^{3+}) [22,23], white LEDs (e.g., $NaBiF_4$:Eu^{3+} and BiF_3:Eu^{3+}) [24,25] and optical thermometry (e.g., BiF_3:Yb^{3+},Er^{3+}) [26]. Recently, $K_{0.3}Bi_{0.7}F_{2.4}$ is emerging as a more attractive host matrix for lanthanide doping to realize tunable emissions in a single phosphor. For instance, An et al. synthesized a series of Yb^{3+}/Ln^{3+} (Ln = Er, Ho, Tm) co-doped $K_{0.3}Bi_{0.7}F_{2.4}$: upconverting nanoparticles for dual-modal in vivo imaging through a solvothermal method at 200 °C for 10 h in ethylene glycol [27]. Gao et al. reported a room-temperature chemical precipitation method to synthesize $K_{0.3}Bi_{0.7}F_{2.4}$:Yb^{3+}, $Er^{3+,}$ and $K_{0.3}Bi_{0.7}F_{2.4}$:Eu^{3+} nanoparticles by using ethylene glycol as the reaction solvent [28,29]. Du et al. have used a similar precipitation method to prepare Tb^{3+}/Eu^{3+}-codoped $K_{0.3}Bi_{0.7}F_{2.4}$ nanoparticles for white LED application [30]. In our previous research, we synthesized the Yb^{3+}/Ln^{3+} (Ln = Er, Ho, Tm)-doped $K_{0.3}Bi_{0.7}F_{2.4}$ nanoparticles by using a very fast (1 min only) method in a water-based system at very low temperature (room temperature−90 °C) [31]. However, rapid synthesis of other lanthanide ions (Pr^{3+}, Nd^{3+}, Sm^{3+}, Dy^{3+}, $Eu^{3+,}$ and Tb^{3+}) doped KBF nanocrystals in the water-based system and their photoluminescence properties are rarely reported.

Here we report the controlled synthesis and multicolor luminescence properties of KBF:Ln nanophosphors synthesized by a low-temperature water-based precipitation method. The composition and morphologies of the obtained KBF:Ln nanophosphors are investigated in detail by varying the synthesis conditions. The obtained KBF:Ln nanophosphors show tunable emission colors and good chemical stability against humidity. The results suggest that the as-prepared KBF:Ln nanophosphors are promising candidates for application in white LEDs and optical thermometry.

2. Experimental Process

$BiCl_3$ (Macklin, Shanghai, China), KF (99.9%, Macklin, Shanghai, China), HCl (37 wt%, Sinopharm, Shanghai, China), $PrCl_3{\cdot}6H_2O$ (99.99%, Aladdin, Shanghai, China), $NdCl_3{\cdot}6H_2O$ (99.9%, Aladdin, Shanghai, China), $SmCl_3{\cdot}6H_2O$ (99.99%, Aladdin, Shanghai, China), $DyCl_3{\cdot}6H_2O$ (99.99%, Aladdin, Shanghai, China), $EuCl_3{\cdot}6H_2O$ (99.99%, Aladdin, Shanghai, China) and $TbCl_3{\cdot}6H_2O$ (99.9%, Aladdin, Shanghai, China) are used as the starting materials. The pure and doped KBF samples were synthesized by a low-temperature water-based precipitation method in accordance with our earlier study [31]. The detailed synthesis procedure and sample characterization are presented in the Supporting Information.

3. Results and Discussion

3.1. Phase Composition of the Pure and Doped KBF Nanocrystals

The phase composition of the prepared pure KBF nanocrystals is first checked by XRD. XRD patterns of the as-prepared non-doped KBF hosts at room temperature are depicted in Figure 1. When the ratios of F/Bi are 4 and 8, the XRD patterns of the obtained samples can be well matched with the corresponding standard XRD data of the cubic $K_{0.3}Bi_{0.7}F_{2.4}$ (JCPDS No. 84–0534), as presented in Figure 1a. The narrow and strong XRD peaks reveal that the pure KBF nanocrystalline particles are highly crystalline. However, as the ratio of F/Bi reaches 12 or higher, it is found that the impurity phase starts to appear at around 27°, assigned to the hexagonal $KBiF_4$ (JCPDS No. 37–0972). Meanwhile, when the F/Bi ratio is set to 8, all the XRD results of the pure KBF nanocrystals obtained at different temperatures (room temperature, 50 °C, and 80 °C) are consistent with the standard pattern of $K_{0.3}Bi_{0.7}F_{2.4}$ crystal, as shown in Figure 1b, indicating that pure KBF can be synthesized in the water-based system at very low temperature. Furthermore, the full width at half-maximum (FWHM) with the dominant XRD peak at 26° presents a declining trend with the increase of reaction temperature, illuminating that the degree of crystallization becomes better for pure KBF nanocrystalline particles at a high synthetic temperature.

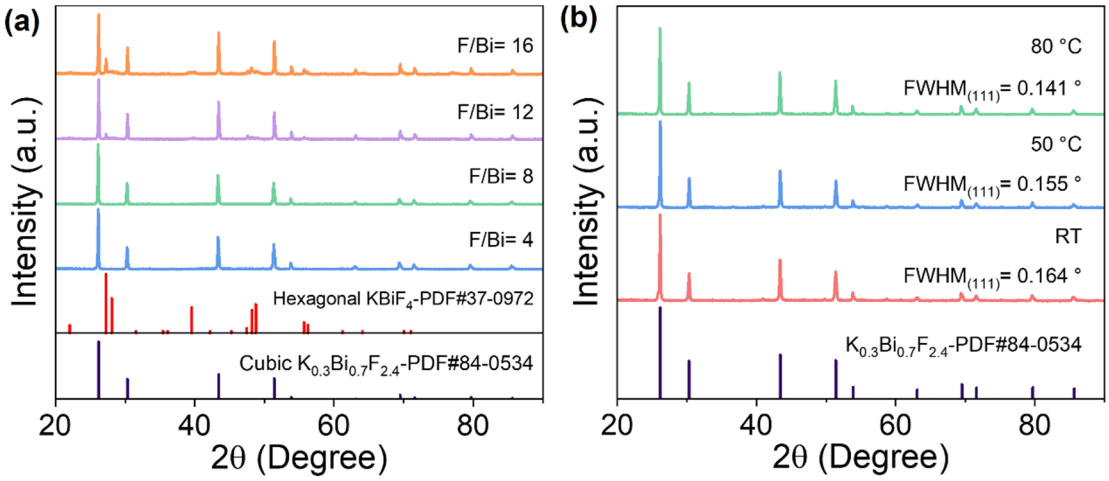

Figure 1. XRD patterns of pure KBF synthesized at different F/Bi ratios (**a**) and reaction temperatures (**b**).

Figure 2 presents the XRD results of the KBF:Ln^{3+} (Ln = Pr, Nd, Sm, Dy, Eu, and Tb) nanocrystalline particles. It can be noted that the XRD patterns of the doped KBF nanocrystals are consistent with the cubic $K_{0.3}Bi_{0.7}F_{2.4}$ compound, which suggests that introducing different lanthanide ions will not lead to the formation of an impurity phase. Meanwhile, the KBF host matrix can accommodate a high concentration of Ln^{3+} (e.g., 25%Eu^{3+} and 30%Tb^{3+}) without changing its crystal structure, indicating that KBF is an attractive host for Ln^{3+} doping to obtain tunable luminescence properties. Furthermore, the average size of KBF:Ln nanocrystalline particles can be estimated by using the Debye Scherrer equation. And the crystallite sizes of KBF:30%Tb, KBF:25%Eu, KBF:5%Dy, KBF:5%Sm, KBF:2%Nd and KBF:5%Pr are calculated to be 20.41, 28.31, 39.75, 45.94, 50.87 and 44.98 nm, respectively.

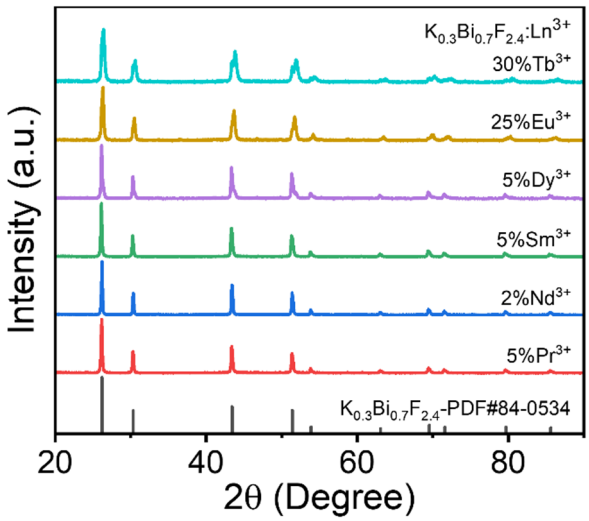

Figure 2. XRD patterns of the doped KBF nanocrystals.

3.2. Morphology Characterization of Pure and Doped KBF Nanocrystalline Particles

The SEM graphs can present the particle size and typical morphology of the as-prepared pure and doped KBF nanocrystals directly and vividly. Figure 3 depicts the representative morphologies of the non-doped KBF nanocrystals synthesized at different ratios of F/Bi. Note that the reaction temperature is room temperature. As presented in Figure 3a,b, when the ratios of F/Bi are determined to be 4 and 8, the obtained pure KBF presents a regular cube shape, and the average size of the cubes decreases as the F/Bi ratio

increases. However, as the ratio value of F/Bi increases to 12 or 16, the morphology of the obtained nanocrystalline particles changes from a cubic shape to an irregular polyhedron. These results indicate that the F/Bi ratio significantly affects the morphology of the final products.

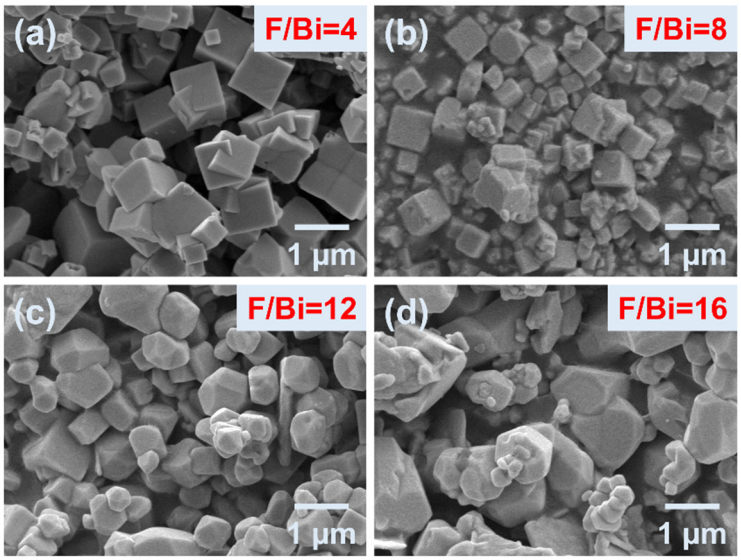

Figure 3. SEM photographs of the pure KBF nanocrystals synthesized at different ratios of F/Bi, (**a**) F/Bi = 4; (**b**) F/Bi = 8; (**c**) F/Bi = 12; (**d**) F/Bi = 16.

Figure 4 presents the SEM graphs of the KBF nanocrystals obtained at different synthetic temperatures. The F/Bi ratio is set to 8. As the reaction temperature increases from room temperature to 80 °C, the cubic morphology of the samples remains almost unchanged, but it is found that the average particle size of the cubic particles increases slightly with an increase in the synthetic temperature.

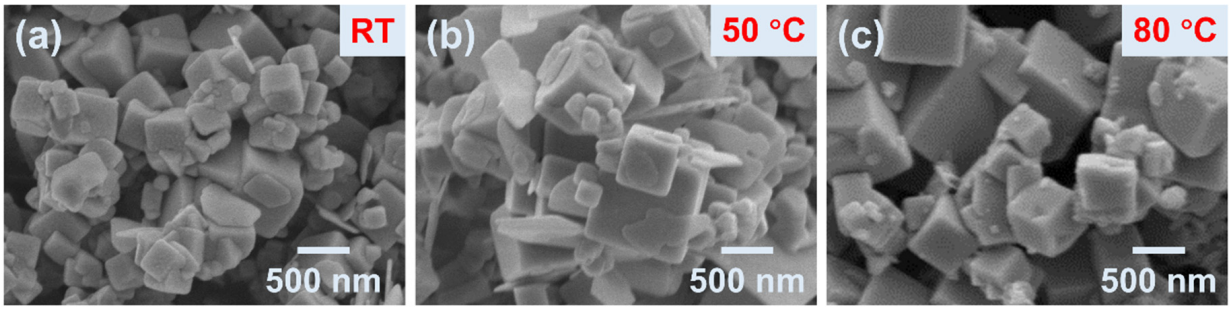

Figure 4. SEM photographs of pure KBF nanocrystals obtained at different synthetic temperatures, (**a**) room temperature; (**b**) T = 50 °C; (**c**) T = 80 °C.

The SEM images of the KBF:Ln (Ln = Pr, Nd, Sm, Dy, Eu, and Tb) nanocrystalline particles synthesized at room temperature are given in Figure 5. When the ratio of F/Bi is determined to be 8, all the as-prepared KBF:Ln samples consist of cubic particles and irregular nanoparticles attached to cubes after introducing different lanthanide ions into the KBF lattice. Compared with the non-doped KBF, the as-prepared KBF:Ln nanocrystalline particles significantly decrease in size. Moreover, the proportion of nanoparticles shows an increasing trend, and the content of cubic particles gradually decreases with an increase in the doping concentration of Ln^{3+}.

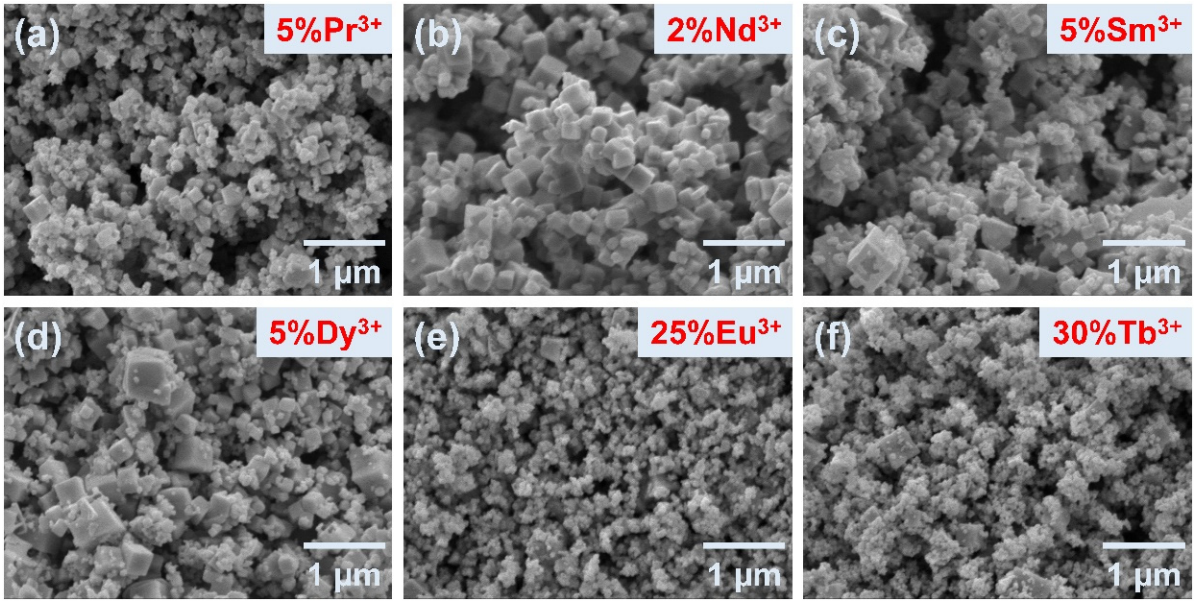

Figure 5. SEM images of the KBF:Ln (Ln = Pr, Nd, Sm, Dy, Eu, and Tb) nanocrystalline particles synthesized at room temperature, introducing (**a**) 5% Pr^{3+}; (**b**) 2% Nd^{3+}; (**c**) 5% Sm^{3+}; (**d**) 5% Dy^{3+}; (**e**) 25% Eu^{3+}; (**f**) 25% Tb^{3+}.

3.3. Photoluminescence Properties of KBF:Ln Nanophosphors

The concentration-dependent emission spectra of KBF:Eu and KBF:Tb nanocrystals are presented in Figure S1. And the optimum doping concentration of Eu^{2+} and Tb^{3+} is determined to be 25% and 30%, respectively. The photoluminescence excitation and emission spectra of KBF:25%Eu are given in Figure 6a. The emission spectrum of KBF:Eu consists of a group of sharp lines at 578, 592, 612, 651, and 700 nm upon 393 nm near-UV light excitation, which can be attributed to the characteristic $^5D_0 \rightarrow {}^7F_J$ (J = 0, 1, 2, 3, 4) electron transitions of Eu^{3+} ions, respectively [32]. Among these emission bands, the most intense one, peaking at 612 nm, originates from the Eu^{3+} $^5D_0 \rightarrow {}^7F_2$ electric-dipole transition. The excitation spectrum monitored at 612 nm emission is made up of multiple excitation bands centered at 362, 376, 393, and 414 nm due to the electron transitions from the $^7F_0$ ground state to the $^5D_4$, $^5G_3$, $^5L_6$, and $^5D_3$ excited levels. Figure 6d shows the excitation and emission spectra of KBF:30%Tb nanocrystalline particles. The emission spectrum exhibits four distinct peaks at 487, 544, 582, and 622 nm when excited by 368 nm of UV light, resulting from the $^5D_4 \rightarrow {}^7F_J$ (J = 6, 5, 4, 3) electron transitions of Tb^{3+} ions, respectively [33]. And the most prominent emission peak is located at 544 nm, assigned to the $^5D_4 \rightarrow {}^7F_5$ transition of Tb^{3+}. The excitation spectrum monitored 544 nm emission comprises excitation bands at 318, 350, and 368 nm due to the $^7F_6 \rightarrow {}^5D_{1,0}$, $^7F_6 \rightarrow {}^5G_{6\text{-}2,}$ and $^7F_6 \rightarrow {}^5D_{2,3}$ transitions of Tb^{3+} ions. Furthermore, it is found that the photoluminescence intensities of KBF:Eu and KBF:Tb nanocrystals decrease gradually with increasing the test temperature from room temperature to 210 °C, which can be attributed to the increase in the non-radiative transition probability, as shown in Figure S2.

To further reveal the chemical stability of the prepared KBF:Ln nanocrystalline particles, the emission spectra of KBF:25%Eu and KBF:30%Tb phosphor powders immersed in deionized water for different days (0, 15, and 30 days) are shown in Figure 6b,e. It can be noticed that the photoluminescence intensity of both KBF:25%Eu and KBF:30%Tb nanophosphors remains almost unchanged under different soaking times in water, indicating that the as-prepared nanophosphors show excellent chemical stability against water.

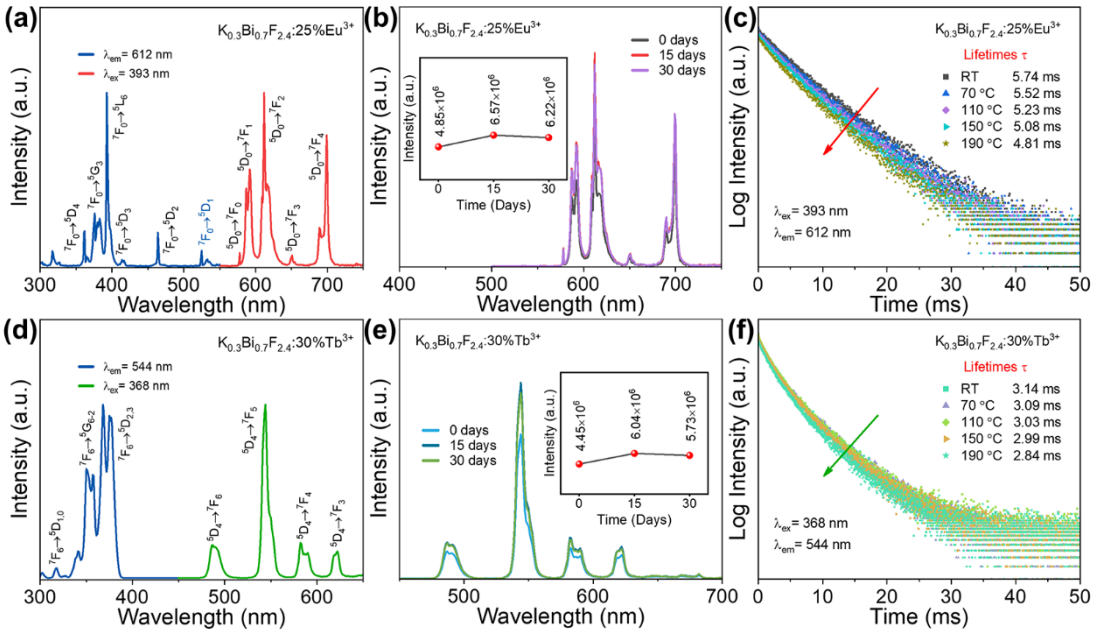

Figure 6. Photoluminescence properties of KBF:25%Eu (**a**–**c**) and KBF:30%Tb nanocrystalline particles (**d**–**f**).

Luminescence decay curves of KBF:25%Eu and KBF:30%Tb samples are depicted in Figure 6c,f. The decay curves can be fitted with a single exponential equation [34]:

$$I(t) = I_0 \exp(-t/\tau) \quad (1)$$

where *I(t)* and I_0 represent the photoluminescence intensity at time t and the background intensity for the dark current of the detector, and τ is the lifetime. Therefore, the average lifetimes of KBF:25%Eu were estimated to be 5.74, 5.52, 5.23, 5.08, and 4.81 ms at different testing temperatures, while the average lifetimes of KBF:30%Tb were determined to be 3.14, 3.09, 3.03, 2.99 and 2.84 ms at different temperatures. For both KBF:25%Eu and KBF:30%Tb samples, the lifetimes show a decreasing trend with the increase of the test temperature, which can be attributed to the increase in the probability of non-radiative transition at high temperature [35]. In addition, the internal quantum efficiencies of KBF:25%Eu and KBF:30%Tb nanocrystals are measured to be 42.39% and 13.75%, respectively (Figure S3). The obtained quantum efficiency values of KBF:25%Eu and KBF:30%Tb samples are comparable with that of the previous reported fluorides, such as $K_{0.3}Bi_{0.7}F_{2.4}$:40%Eu^{3+} (14.9%) [29] and $K_{0.3}Bi_{0.7}F_{2.4}$:9%Tb^{3+},0.6%Eu^{3+} (50.8%) [30].

The photoluminescence emission and excitation spectra of the KBF:Ln^{3+} (Ln = Pr, Nd, Sm, Dy) nanocrystals are depicted in Figure 7. As presented in Figure 7a, the excitation spectrum of KBF:5%Pr nanocrystal monitored at 606 nm emission is composed of three distinct excitation bands centered at 443, 467, and 481 nm, which are caused by the characteristic $^3H_4 \rightarrow {}^3P_J$ (J = 0, 1, 2) electron transitions of Pr^{3+} ions, respectively [36]. The emission spectrum with a dominant peak at 606 nm in a wavelength range over 500–750 nm can be assigned to the Pr^{3+} $^1D_2 \rightarrow {}^3H_4$ transition [37]. The emission spectrum of KBF:2%Nd, upon 808 nm excitation, shows three emission bands at 870, 1054, and 1325 nm. This can be attributed to the characteristic $^4F_{3/2} \rightarrow {}^4I_{9/2}$, $^4F_{3/2} \rightarrow {}^4I_{11/2}$ and $^4F_{3/2} \rightarrow {}^4I_{13/2}$ transitions of Nd^{3+}, respectively, as shown in Figure 7b, while its excitation spectrum is made up of a group of sharp lines in the visible and NIR regions arising from intraconfigurational f-f transitions of Nd^{3+} [38]. Figure 7c gives the photoluminescence properties of the yielded KBF:5%Sm nanocrystalline particles. The emission spectrum shows several distinct bands centered at 559, 595, 641, and 700 nm ascribed to the $^4G_{5/2} \rightarrow {}^6H_J$ (J = 5/2, 7/2, 9/2, and 11/2) transitions of Sm^{3+} ions upon 399 nm excitation, respectively [36]. The excitation

spectrum of KBF:5%Sm monitored at 595 nm emission spans from 300 to 500 nm with a dominant excitation peak at 399 nm ascribed to the $^6H_{5/2} \rightarrow {}^4K_{11/2}$ electron transition of Sm^{3+} [39]. Figure 7d depicts the photoluminescence properties of KBF:5%Dy nanocrystals. The excitation spectrum monitored at 572 nm emission is composed of a group of narrow excitation bands in the UV assigned to the electron transitions from $^6H_{15/2}$ to $^6P_{3/2}$, $^6P_{7/2}$, $^6P_{5/2,}$ and $^4I_{13/2}$ excited levels of Dy^{3+} ions, respectively [40]. Under the excitation of 364 nm, the emission spectrum exhibits four distinct bands with a maximum emission peak of 572 nm due to the Dy^{3+} $^4F_{9/2} \rightarrow {}^6H_{13/2}$ transition. Overall, the emission colors of the as-prepared nanocrystals can be finely tuned by doping different Ln^{3+} in a single KBF host.

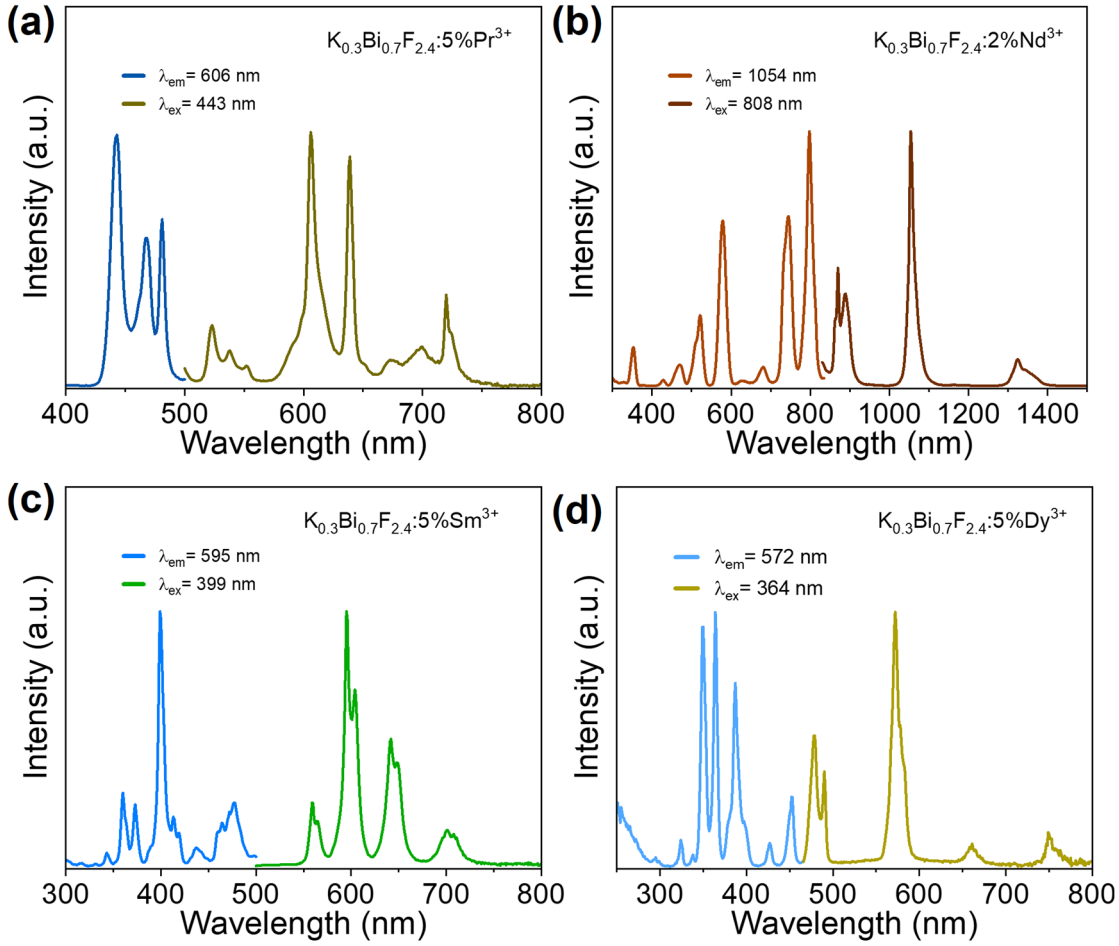

Figure 7. Photoluminescence properties of KBF:Ln (Ln = Pr, Nd, Sm, Dy) nanocrystalline particles (**a**–**d**).

4. Conclusions

In conclusion, we have successfully prepared pure and doped KBF nanocrystalline particles via a rapid water-based precipitation route. With varying the ratios of F/Bi and reaction temperatures, the morphology of samples can be tuned from cubic shape to irregular polyhedron. The as-prepared KBF:Ln (Ln = Pr, Nd, Sm, Dy, Eu, and Tb) nanophosphors exhibit intense characteristic photoluminescence from the electron transitions of the doped trivalent lanthanides. Meanwhile, the morphology and photoluminescence performance of these KBF:Ln nanophosphors remain almost unchanged even when immersed in water for 30 days, indicating the obtained KBF:Ln samples have excellent chemical stability. The merit of multicolor luminescence in these KBF:Ln nanocrystalline particles holds great promise when applied to a wide range of important fields, such as optoelectronic devices and optical thermometry.

Supplementary Materials: The following supporting information can be downloaded at: https://www.mdpi.com/article/10.3390/cryst12070963/s1, Figure S1: Emission spectra of the KBF:Ln (Ln = Eu, Tb) samples doped with different Ln^{3+} concentrations; Figure S2: temperature-dependent emission spectra of the KBF:25%Eu (a) and KBF:30%Tb (b) samples; Figure S3: Excitation line of $BaSO_4$ and emission spectrum of KBF:25%Eu (a) and KBF:30%Tb (b) samples. Inset shows the magnification of the emission spectrum. Table S1:The crystallite size of pure KBF synthesized at different reaction temperatures. Table S2: The crystallite size of the lanthanide doped KBF nanocrystalline particles.

Author Contributions: Conceptualization, W.W., S.M., D.C. and Y.L.; methodology, W.W., S.M. and D.C.; software, S.M. and D.C.; validation, W.W. and Y.L.; data curation, S.M. and D.C.; writing—original draft preparation, W.W., S.M., D.C. and Y.L.; writing—review and editing, Y.L. All authors have read and agreed to the published version of the manuscript.

Funding: This work was financially supported by the National Natural Science Foundation of China (Grant No. 51902184), Key Research and the Development Program of Shandong Province (Major Scientific and Technological Innovation Project) (Grant No. 2021CXGC011101), the Natural Science Foundation of Shandong Province (Grant Nos. ZR2019BEM028 and ZR2020ME028) and the "Qi-Lu Young Scholar Fund" (Grant No. 31370088963167) from Shandong University.

Institutional Review Board Statement: Not applicable.

Informed Consent Statement: Not applicable.

Data Availability Statement: All supporting and actual data are presented in the manuscript.

Conflicts of Interest: The authors declare they have no known competing financial interests or personal relationships that could appear to influence the work reported in this paper.

References

1. Terraschke, H.; Wickleder, C. UV, blue, green, yellow, red, and small: Newest developments on Eu^{2+}-doped nanophosphors. *Chem. Rev.* **2015**, *115*, 11352–11378. [CrossRef] [PubMed]
2. Algar, W.R.; Massey, M.; Rees, K.; Higgins, R.; Krause, K.D.; Darwish, G.H.; Peveler, W.J.; Xiao, Z.; Tsai, H.Y.; Gupta, R.; et al. Photoluminescent nanoparticles for chemical and biological analysis and imaging. *Chem. Rev.* **2021**, *121*, 9243–9358. [CrossRef] [PubMed]
3. Ren, W.; Lin, G.; Clarke, C.; Zhou, J.; Jin, D. Optical nanomaterials and enabling technologies for high-security-level anticounterfeiting. *Adv. Mater.* **2020**, *32*, 1901430. [CrossRef] [PubMed]
4. Kim, H.; Beack, S.; Han, S.; Shin, M.; Lee, T.; Park, Y.; Kim, K.S.; Yetisen, A.K.; Yun, S.H.; Kwon, W.; et al. Multifunctional photonic nanomaterials for diagnostic, therapeutic, and theranostic applications. *Adv. Mater.* **2018**, *30*, 1701460. [CrossRef] [PubMed]
5. Chen, D.; Zhang, L.; Liang, Y.; Wang, W.; Yan, S.; Bi, J.; Sun, K. Yolk–shell structured Bi_2SiO_5:Yb^{3+},Ln^{3+} (Ln = Er, Ho, Tm) upconversion nanophosphors for optical thermometry and solid-state lighting. *CrystEngComm* **2020**, *22*, 4438. [CrossRef]
6. Wang, F.; Liu, X. Multicolor tuning of lanthanide-doped nanoparticles by single wavelength excitation. *Acc. Chem. Res.* **2014**, *47*, 1378–1385. [CrossRef] [PubMed]
7. Zeng, Z.; Huang, B.; Wang, X.; Lu, L.; Lu, Q.; Sun, M.; Wu, T.; Ma, T.; Xu, J.; Xu, Y.; et al. Multimodal luminescent Yb^{3+}/Er^{3+}/Bi^{3+}-doped perovskite single crystals for X-ray detection and anti-counterfeiting. *Adv. Mater.* **2020**, *32*, 2004506. [CrossRef] [PubMed]
8. Xie, X.; Li, Z.; Zhang, Y.; Guo, S.; Pendharkar, A.I.; Lu, M.; Huang, L.; Huang, W.; Han, G. Emerging ≈800 nm excited lanthanide-doped upconversion nanoparticles. *Small* **2017**, *13*, 1602843. [CrossRef] [PubMed]
9. Huang, H.; Chen, J.; Liu, Y.; Lin, J.; Wang, S.; Huang, F.; Chen, D. Lanthanide-doped core@multishell nanoarchitectures: Multimodal excitable upconverting/downshifting luminescence and high-level anti-counterfeiting. *Small* **2020**, *16*, 2000708. [CrossRef]
10. Vetrone, F.; Naccache, R.; Zamarrón, A.; de la Fuente, A.J.; Sanz-Rodríguez, F.; Maestro, L.M.; Rodriguez, E.M.; Jaque, D.; Solé, J.G.; Capobianco, J.A. Temperature sensing using fluorescent nanothermometers. *ACS Nano* **2010**, *4*, 3254–3258. [CrossRef]
11. Zhuang, Y.; Chen, D.; Chen, W.; Zhang, W.; Su, X.; Deng, R.; An, Z.; Chen, H.; Xie, R.J. X-ray-charged bright persistent luminescence in $NaYF_4$:Ln^{3+}@$NaYF_4$ nanoparticles for multidimensional optical information storage. *Light Sci. Appl.* **2021**, *10*, 132. [CrossRef] [PubMed]
12. Mai, H.X.; Zhang, Y.W.; Si, R.; Yan, Z.G.; Sun, L.D.; You, L.P.; Yan, C.H. High-quality sodium rare-earth fluoride nanocrystals: Controlled synthesis and optical properties. *J. Am. Chem. Soc.* **2006**, *128*, 6426–6436. [CrossRef] [PubMed]
13. Gnanasammandhan, M.K.; Idris, N.M.; Bansal, A.; Huang, K.; Zhang, Y. Near-IR photoactivation using mesoporous silica-coated $NaYF_4$:Yb,Er/Tm upconversion nanoparticles. *Nat. Protoc.* **2016**, *11*, 688–713. [CrossRef]
14. Yi, G.S.; Chow, G.M. Synthesis of hexagonal-phase $NaYF_4$:Yb,Er and $NaYF_4$:Yb,Tm nanocrystals with efficient up-conversion fluorescence. *Adv. Funct. Mater.* **2006**, *16*, 2324–2329. [CrossRef]

15. Liu, D.; Xu, X.; Du, Y.; Qin, X.; Zhang, Y.; Ma, C.; Wen, S.; Ren, W.; Goldys, E.M.; Piper, J.A.; et al. Three-dimensional controlled growth of monodisperse sub-50 nm heterogeneous nanocrystals. *Nat. Commun.* **2016**, *7*, 10254. [CrossRef] [PubMed]
16. Mohan, R. Green bismuth. *Nat. Chem.* **2010**, *2*, 336. [CrossRef] [PubMed]
17. Swart, H.C.; Kroon, R.E. Ultraviolet and visible luminescence from bismuth doped materials. *Opt. Mater. X* **2019**, *2*, 100025. [CrossRef]
18. Zhou, Z.; Wang, X.; Yi, X.; Ming, H.; Ma, Z.; Peng, M. Rechargeable and sunlight-activated $Sr_3Y_2Ge_3O_{12}$:Bi^{3+} UV–Visible-NIR persistent luminescence material for night-vision signage and optical information storage. *Chem. Eng. J.* **2021**, *421*, 127820. [CrossRef]
19. Zeng, Z.; Sun, M.; Zhang, S.; Zhang, H.; Shi, X.; Ye, S.; Huang, B.; Du, Y.; Yan, C.H. Rare-earth-based perovskite $Cs_2AgScCl_6$:Bi for strong full visible spectrum emission. *Adv. Funct. Mater.* **2022**, 2204780. [CrossRef]
20. Lei, P.; An, R.; Yao, S.; Wang, Q.; Dong, L.; Xu, X.; Du, K.; Feng, J.; Zhang, H. Ultrafast synthesis of novel hexagonal phase $NaBiF_4$ upconversion nanoparticles at room temperature. *Adv. Mater.* **2017**, *29*, 1700505. [CrossRef]
21. Back, M.; Ueda, J.; Ambrosi, E.; Cassandro, L.; Cristofori, D.; Ottini, R.; Riello, P.; Sponchia, G.; Asami, K.; Tanabe, S.; et al. Lanthanide-doped bismuth-based fluoride nanocrystalline particles: Formation, spectroscopic investigation, and chemical stability. *Chem. Mater.* **2019**, *31*, 8504–8514. [CrossRef]
22. Saraf, R.; Shivakumara, C.; Behera, S.; Dhananjaya, N.; Nagabhushana, H. Synthesis of Eu^{3+}-activated BiOF and BiOBr phosphors: Photoluminescence, Judd–Ofelt analysis and photocatalytic properties. *RSC Adv.* **2015**, *5*, 9241–9254. [CrossRef]
23. Wei, D.; Huang, Y.; Seo, H.J. Eu^{3+}-doped $Bi_7O_5F_{11}$ microplates with simultaneous luminescence and improved photocatalysis. *APL Mater.* **2020**, *8*, 081109. [CrossRef]
24. Du, P.; Huang, X.; Yu, J.S. Facile synthesis of bifunctional Eu^{3+}-activated $NaBiF_4$ red-emitting nanoparticles for simultaneous white light-emitting diodes and field emission displays. *Chem. Eng. J.* **2018**, *337*, 91–100. [CrossRef]
25. Sarkar, S.; Dash, A.; Mahalingam, V. Strong stokes and upconversion luminescence from ultrasmall Ln^{3+}-doped BiF_3 (Ln = Eu^{3+}, Yb^{3+}/Er^{3+}) nanoparticles confined in a polymer matrix. *Chem. Asian J.* **2014**, *9*, 447–451. [CrossRef]
26. Zhao, S.; Tian, R.; Shao, B.; Feng, Y.; Yuan, S.; Dong, L.; Zhang, L.; Wang, Z.; You, H. One-pot synthesis of Ln^{3+}-doped porous BiF_3@PAA nanospheres for temperature sensing and pH-responsive drug delivery guided by CT imaging. *Nanoscale* **2020**, *12*, 695–702. [CrossRef]
27. An, R.; Lei, P.; Zhang, P.; Xu, X.; Feng, J.; Zhang, H. Near-infrared optical and X-ray computed tomography dual-modal imaging probe based on novel lanthanide-doped $K_{0.3}Bi_{0.7}F_{2.4}$ upconversion nanoparticles. *Nanoscale* **2018**, *10*, 1394–1402. [CrossRef] [PubMed]
28. Gao, X.; Song, F.; Ju, D.; Zhou, A.; Khan, A.; Chen, Z.; Sang, X.; Feng, M.; Liu, L. Room-temperature ultrafast synthesis, morphology and upconversion luminescence of $K_{0.3}Bi_{0.7}F_{2.4}$:Yb^{3+}/Er^{3+} nanoparticles for temperature-sensing application. *CrystEngComm* **2020**, *22*, 7066–7074. [CrossRef]
29. Gao, X.; Song, F.; Khan, A.; Chen, Z.; Ju, D.; Sang, X. Room temperature synthesis, Judd Ofelt analysis and photoluminescence properties of down-conversion $K_{0.3}Bi_{0.7}F_{2.4}$:Eu^{3+} orange red phosphors. *J. Lumin.* **2021**, *230*, 117707. [CrossRef]
30. Du, P.; Wan, X.; Luo, L.; Li, W.; Li, L. Thermally stable Tb^{3+}/Eu^{3+}-codoped $K_{0.3}Bi_{0.7}F_{2.4}$ nanoparticles with multicolor luminescence for white-light-emitting diodes. *ACS Appl. Nano Mater.* **2021**, *4*, 7062–7071. [CrossRef]
31. Chen, D.; Bi, J.; Wang, W.; Wang, X.; Zhang, Y.; Liang, Y. Rapid aqueous-phase synthesis of highly stable $K_{0.3}Bi_{0.7}F_{2.4}$ upconversion nanocrystalline particles at low temperature. *Inorg. Chem. Front.* **2021**, *8*, 1039–1048. [CrossRef]
32. Chen, D.; Miao, S.; Liang, Y.; Wang, W.; Yan, S.; Bi, J.; Sun, K. Controlled synthesis and photoluminescence properties of Bi_2SiO_5:Eu^{3+} core-shell nanospheres with an intense $^5D_0 \rightarrow {}^7F_4$ transition. *Opt. Mater. Express* **2021**, *11*, 355–370. [CrossRef]
33. Wang, Y.; Chen, D.; Zhuang, Y.; Chen, W.; Long, H.; Chen, H.; Xie, R.J. $NaMgF_3$:Tb^{3+}@$NaMgF_3$ nanoparticles containing deep traps for optical information storage. *Adv. Opt. Mater.* **2021**, *9*, 2100624. [CrossRef]
34. Zhang, Y.; Miao, S.; Liang, Y.; Liang, C.; Chen, D.; Shan, Z.; Sun, K.; Wang, X.J. Blue LED-pumped intense short-wave infrared luminescence based on Cr^{3+}-Yb^{3+}-codoped phosphors. *Light Sci. & Appl.* **2022**, *11*, 136.
35. Yuan, C.; Li, R.; Liu, Y.; Zhang, L.; Zhang, J.; Leniec, G.; Sun, P.; Liu, Z.; Luo, Z.; Dong, R.; et al. Efficient and broadband $LiGaP_2O_7$:Cr^{3+} phosphors for smart near-infrared light-emitting diodes. *Laser Photonics Rev.* **2021**, *15*, 2100227. [CrossRef]
36. Liang, Y.; Liu, F.; Chen, Y.; Wang, X.; Sun, K.; Pan, Z. Red/near-infrared/short-wave infrared multi-band persistent luminescence in Pr^{3+}-doped persistent phosphors. *Dalton Trans.* **2017**, *46*, 11149–11153. [CrossRef]
37. Wang, B.; Lin, H.; Xu, J.; Chen, H.; Lin, Z.; Huang, F.; Wang, Y. Design, preparation, and characterization of a novel red long-persistent perovskite phosphor: $Ca_3Ti_2O_7$:Pr^{3+}. *Inorg. Chem.* **2015**, *54*, 11299–11306. [CrossRef]
38. Chen, D.; Liang, Y.; Miao, S.; Bi, J.; Sun, K. Nd^{3+}-doped Bi_2SiO_5 nanospheres for stable ratiometric optical thermometry in the first biological window. *J. Lumin.* **2021**, *234*, 117967. [CrossRef]
39. Li, Y.C.; Chang, Y.H.; Lin, Y.F.; Chang, Y.S.; Lin, Y.J. Synthesis and luminescent properties of Ln^{3+} (Eu^{3+}, Sm^{3+}, Dy^{3+})-doped lanthanum aluminum germanate $LaAlGe_2O_7$ phosphors. *J. Alloys Compd.* **2007**, *439*, 367–375. [CrossRef]
40. Tian, T.; Feng, H.; Zhang, Y.; Zhou, D.; Shen, H.; Wang, H.; Xu, J. Crystal growth and luminescence properties of Dy^{3+} and Ge^{4+} co-doped $Bi_4Si_3O_{12}$ single crystals for high power warm white LED. *Crystals* **2017**, *7*, 249. [CrossRef]